Active Ester Functional Single Core Magnetic Nanostructures as a Versatile Immobilization Matrix for Effective Bioseparation and Catalysis

Thorsten Gelbrich,[†] Michael Reinartz,[‡] and Annette M. Schmidt*[,†]

Institut für Organische Chemie und Makromolekulare Chemie, and Institut für Herz- und Kreislaufphysiologie, Heinrich-Heine-Universität Düsseldorf, Universitätsstr. 1, D-40225 Düsseldorf, Germany

Received October 22, 2009; Revised Manuscript Received January 10, 2010

Multifunctional nanocarriers for amino functional targets with a high density of accessible binding sites are obtained in a single polymerization step by grafting from copolymerization of an active ester monomer from superparamagnetic cores. As a result of the brush-like structure of the highly dispersed shell, the nano-objects exhibit an available capture capacity for amines that is found to be up to 2 orders of magnitude higher than for commercial magnetic beads, and the functional brush shell can serve as a template for many types of pendant functional groups and molecules. As comonomer, oligo(ethylene glycol) methacrylate allows for excellent water solubility at room temperature, biocompatibility, and thermoflocculation. We demonstrate the biorelated applicability of the hybrid nanoparticles by two different approaches. In the first approach, the immobilization of trypsin to the core−shell nanoparticles results in highly active, nanoparticulate biocatalysts that can easily be separated magnetically. Second, we demonstrate that the obtained nanoparticles are suitable for the effective labeling of cell membranes, opening a novel pathway for the easy and effective isolation of membrane proteins.

Introduction

Using colloidal supports for bioactive species has enabled important advances in biotechnology, medical diagnostics, drug screening, and other areas of actual interest. In in vitro as well as in in vivo environments, the substrate can introduce or facilitate the feasibility to detect, quantify, localize, or separate biologically active species.

In this respect, superparamagnetic carriers actually attract high attention as they enable the visualization, manipulation, and activation of labeled species by the use of properly designed magnetic fields. Examples for the wide applicability of magnetic colloids in the bioscience include contrast agents for MRI, magnetic separation kits, and therapeutic approaches like magnetic fluid hyperthermia and active drug delivery.[1−6]

When designing an immobilization matrix, a range of factors such as density and accessibility of binding sites, their microenvironment, and mobility strongly influence the intensity of interaction and the effectiveness of the binding event.[7] In this respect, the question of size relevance is nontrivial. In general, small carriers in the nanometer range are superior in terms of accessible surface, their mode of interaction with cells and proteins, and higher mobility with respect to diffusion and cell uptake. In contrast, concerning the ease of detection and separation, micrometer-sized solid supports have clear advantages over smaller structures and show higher effectivity for their isolation by centrifugation or filtering methods. In the case of magnetic structures, micrometer-sized beads can possess a higher magnetic moment, thus, enhancing magnetophoretic mobility, magnetic contrast, and heatability in HF fields.

Reversible thermoflocculation of magnetic colloids by encapsulation with thermoresponsive polymers as a strategy to overcome this gap has been proposed already in the 90s.[8] While latexes or microgels containing magnetic nanoparticles are relatively easy to disperse at the application temperature, they possess agglomeration at a temperature range above or below, caused by a thermosensitive solvation behavior of the polymer component. As the latter, poly(*N*-isopropylacrylamide) PNiPAAm is frequently employed,[8−10] although the LCST-type flocculation temperature of 32 °C does not allow good particle dispersion at body temperature, and furthermore, the polymer tends to unspecific protein adsorption. As an alternative, just recently, beads based on acryloyl glycinamide copolymers with UCST behavior that flocculate below 10 °C have been developed and commercialized.[11,12]

To provide an increased versatility in terms of protein interaction, thermal behavior, and particle mobility, hydrophilic coatings with controlled polymer architecture and easily tunable parameters are needed. The formation of a polymer brush on the surface of single nanoparticles has proved to be a valuable tool for the design of single-cored hybrid structures with tailored dispersion behavior.[9,13−19] The advances of a brush shell architecture are a high density of end-tethered chains, a shell thickness that is adjustable by the polymer arm length, and a greatly increased accessibility of the chains by solvent molecules and reactants as compared to latex beads or cross-linked microgels. Magnetic polymer brushes with thermoflocculation behavior have been reported for organic solvents by our group.[17−19] Lately, hydrophilic brush shells have been described,[20,21] for instance, prepared by a "grafting to" approach of tailored copolymers from oligo(ethylene glycol) methacrylates with adjustable and narrow flocculation temperature and low unspecific adsorption.[22,23]

Here, we report the design and application of single-cored hybrid magnetic core−shell particles that carry a high number

* To whom correspondence should be addressed. Phone: +49-211-8114820. Fax: +49-211-15840. E-mail: schmidt.annette@uni-duesseldorf.de.
[†] Institut für Organische Chemie und Makromolekulare Chemie.
[‡] Institut für Herz- und Kreislaufphysiologie.

10.1021/bm901203z
Published on Web 02/04/2010

Table 1. Composition of the Investigated FeO_x−P(OEGMA-*co*-SIMA) Core-Shell Nanoparticles[a]

sample[a]	μ_P (%)	M_s (A·m^{-1})	μ_{MF} (%)	d_c (nm)	d_h (nm)	T_c (°C)
FeO_x−P(OEGMA-*co*-SIMA)25	40.4	2090	2.14	12.1	79	59.4
FeO_x−P(OEGMA-*co*-SIMA)20	49.9	1520	1.54	10.3	47	57.8
FeO_x−P(OEGMA-*co*-SIMA)15	41.3	2280	2.33	12.0	73	60.8
FeO_x−P(OEGMA-*co*-SIMA)10	52.1	1490	1.51	10.4	49	57.9
FeO_x−P(OEGMA-*co*-SIMA)5	43.9	1890	1.91	10.4	48	

[a] Sample annotations: FeO_x−P(OEGMA-*co*-SIMA)xy, with xy = theoretical molar SIMA content in the copolymeric shell; μ_P = mass content of copolymer in the particles (EA); M_s = saturation magnetization of saturated DMSO particle dispersions (VSM); μ_{MF} = mass content of FeO_x magnetic cores in saturated DMSO dispersion (VSM); d_c = volume average core diameter (VSM); d_h = hydrodynamic diameter (DLS); T_c = critical solution temperature (cloud point photometry, CPP) of partly hydrolyzed particles.

of reactive groups in a single polymerization step. The polymer brush shells are prepared by a grafting from (surface-initiated) atom transfer radical polymerization. By copolymerization of a monomer with active ester functionality, we are able to introduce a high density of accessible functional groups that facilitate the nucleophilic attack of amine-terminated moieties. This way, not only is the extra functionalization step avoided, but the polymer becomes a template for many types of pendant functional groups and molecules. While the controlled polymerization of active ester monomers in solution has frequently been reported, there are few reports of those polymers grafted from solid surfaces.[24,25] We demonstrate that this strategy results in a high specific number of binding sites, being up to two orders of magnitude higher than for magnetic bead structures.

Their versatile application is demonstrated on two examples. By reacting the active ester-functional moieties with trypsin, we result in magnetically supported biocatalysts for protein scission that provide quasi-homogeneous reaction conditions at body temperature and easy separation at elevated temperatures. Second, the successful capture of membrane proteins by active-ester bearing particles has been demonstrated for endothelial cells in vitro being of use for future applications of membrane protein characterization.

Experimental Section

Analytical Methods and Instrumentation. DLS experiments and zeta potential measurements are performed on a Malvern Zetasizer Nano ZS at 25 °C. ATR-IR spectra are measured on a Nicolet 6700 spectrometer. Vibrating sample magnetometry (VSM) measurements are implemented on an ADE Magnetics vibrating sample magnetometer EV7. For UV/vis spectroscopy a Nicolet UV 540 spectroscope is used. The phase behavior of aqueous particle dispersions is investigated on a Tepper TP1 cloud point photometer at 1 K·min^{-1} in HEPES buffer. Elemental analyses are performed on a Perkin-Elmer 2400 CHN analyzer. The polymer content is calculated through C content. TEM pictures are taken on a Hitachi H 600.

Materials. Benzylamine (BzA; Janssen Chimica), N_α-benzoyl-D,L-arginin-4-nitroanilide hydrochloride (BAPNA; Sigma, 98%), 2,2′-bipyridine (Aldrich, 99%), citric acid monohydrate (Grüssing GmbH, 99,5%), copper(I) bromide (Aldrich, 98%), (4-(chloromethyl)phenyl)-trimethoxysilane (CPTMS; ABCR, 95%), 1-(3-dimethylaminopropyl)-3-ethylcarbodiimide hydrochloride (EDC; ABCR, 98%), iron(III) chloride hexahydrate, iron(II) chloride tetrahydrate (Fluka, 98%), *N*-hydroxysuccinimide (NHS; Aldrich, 98%), ninhydrin (Riedel-de-Haen), oligo(ethylene glycol) methyl ether methacrylate (OEGMA; Aldrich; M_n = 290 g·mol^{-1}), tetramethylammoniumhydroxide aq. (Aldrich, 25%), and trypsin type IX-S (Aldrich) are used as received. Ethanol is obtained in technical grade and used after distillation. Dimethylsulfoxide (DMSO) is dried by heating over calcium hydride (Riedel-de-Haen) for two hours, followed by distillation under reduced pressure. Succinimidyl methacrylate (SIMA) is synthesized by a method by Gatz et al.[26] HEPES buffer was prepared as follows: 11 mM HEPES (Sigma), 140 mM NaCl (Merck), 4 mM KCl (Merck), and 10 mM D(+)-glucose dissolved in deionized water.

Synthesis of CPTMS-Functionalized FeO_x Nanoparticles. Magnetic FeO_x nanoparticles are obtained by alkaline coprecipitation of iron(II) and iron(III) chloride based on a method of Cabuil and Massart.[27] The particles are washed several times with deionized water and then stirred for 5 min with 420 mL of 2 M nitric acid. After three washing steps with nitric acid, the particle precipitate is resuspended in 90 mL of 0.01 M citric acid to functionalize the particle surface with citric acid. Again the nanoparticles are magnetically separated and redispersed by the addition of aqueous tetramethyl ammonium hydroxide (pH 7−8). For the surface modification, the magnetic fluid is added dropwise to a stirred 1.8 mM solution of CPTMS in ethanol up to a concentration of 1 g·L^{-1} FeO_x. After allowing the ligand exchange reaction at ambient temperature overnight, the mixture is concentrated on a rotary evaporator to a 10th of the original volume. The obtained CPTMS functionalized nanoparticles are then magnetically separated from the supernatant and washed five times with a 1:1 mixture of diethyl ether and acetone. Finally, the particle precipitate is redispersed in DMSO for the following surface initiated polymerization.

ATR-IR spectra of dried functionalized FeO_x nanoparticles show several characteristic peaks that are also found in the spectrum of free CPTMS. The vibrational absorption at 1604, 1480, 1259, and 1379 cm^{-1} and a broad signal between 1140 and 850 cm^{-1} confirm the surface functionalization with CPTMS.

Surface Initiated ATR Copolymerization of OEGMA and SIMA. Magnetic FeO_x−P(OEGMA-*co*-SIMA) core−shell nanoparticles are obtained by dissolving CuBr and bpy (1:2.5 mol/mol) in a DMSO-based dispersion of CPTMS functionalized FeO_x nanoparticles (35 mg·L^{-1} FeO_x). OEGMA and SIMA (total monomer content 30 mass %) are added to start the polymerization. The runs are based on two initiator batches that have been analogously prepared as described above, and the composition of the copolymers is chosen to achieve a SIMA content in the polymer shell of 5, 10, and 20 mol % for one initiator batch, and 15 and 25 mol % for the other initiator batch (Table 1). The reaction is carried out for 24 h under stirring at ambient temperature. The obtained core−shell nanoparticles are transferred to buffer-based dispersions by precipitation of the primary DMSO dispersions in diethyl ether, magnetic separation and redispersion in buffer.

Capture of Benzylamine. Five BzA solutions in HEPES-buffer are prepared with concentrations between 20 mM and 2.5 mM. For each of the investigated particle samples (FeO_x−P(OEGMA-*co*-SIMA)20, FeO_x−P(OEGMA-*co*-SIMA)10, and FeO_x−P(OEGMA-*co*-SIMA)5) HEPES buffer-based dispersions with known particle concentrations (FeO_x−P(OEGMA-*co*-SIMA20, 34.9 mg·L^{-1}; FeO_x−P(OEGMA-*co*-SIMA10, 69.8 mg·L^{-1}; FeO_x−P(OEGMA-*co*-SIMA5, 139.6 mg·L^{-1}) are prepared. For the binding experiments 0.5 mL of the respective BzA solution is mixed with 1 mL of the particle dispersion and 0.5 mL of an activation solution composed of 18.73 mM EDC and 43.30 mM NHS and shaken overnight.

Quantitative Analysis of the BzA Residue by Ninhydrin Reaction. To remove the strongly light-absorbing particles from the reaction mixtures for UV analysis, the hybrids are magnetically separated by a Milteny column or by heating above the LCST and the use of a magnet. For the ninhydrin reaction, 1 mL of the respective supernatant is mixed with 1 mL of a 40 mM ethanolic ninhydrin solution in a pressure resistant vial and the vial is closed. The reaction is carried

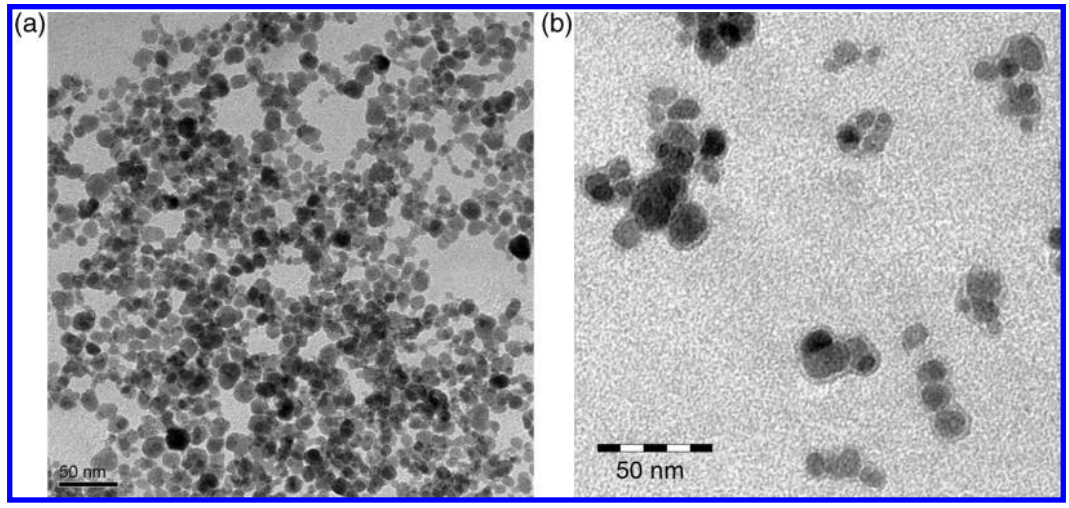

Figure 1. TEM images of (a) FeO_x nanoparticles electrostatically stabilized by citric acid; (b) FeO_x nanoparticles after surface-initiated ATRP.

out under stirring at 100 °C for 20 min. After cooling to ambient temperature, the purple colored solutions are dissolved (1:10 and 1:5, respectively), and the absorption at 568 nm is measured by UV/vis spectroscopy.

Immobilization of Trypsin. Trypsin (30 mg) was dissolved in 6 mL HEPES buffer and mixed with 6 mL of a HEPES buffer-based FeO_x−P(OEGMA-*co*-SIMA)15 particle dispersion ($\mu(FeO_x) = 0.15$ mass %). To allow reactivation of possibly hydrolyzed active-ester functions, 6 mL of 2.21 μM EDC/NHS solution is added. The binding reaction is carried out for 6 h at ambient temperature on a shaker. The obtained trypsin functionalized particles were separated and washed carefully with water to remove any residues of free trypsin and redispersed in HEPES buffer.

Determination of Immobilized Enzyme Kinetics and Activity. BAPNA is used as the model substrate. Four HEPES buffered BAPNA solutions with concentrations between 2.0 and 0.5 mM, and a 6.0 μM trypsin solution are prepared. The respective BAPNA solution is added to a cuvette and mixed with 100 μL of FeO_x−POEGMA-trypsin nanoparticle dispersion or 50 μL trypsin solution. The resulting concentrations of trypsin in the two systems are 9.82×10^{-8} mol·L^{-1} (free trypsin) and 1.66×10^{-7} mol·L^{-1} (FeO_x−POEGMA-trypsin particle dispersion). Directly after addition of the enzyme the change in absorption at 410 nm is detected every 15 or 30 s over a period of up to 20 min by UV spectroscopy.

Functionalization of Endothelial Cell Membranes. Cultured endothelial cells (second passage) from human umbilical cord are incubated with a FeO_x−P(OEGMA-*co*-SIMA)25 and a FeO_x−POEGMA nanoparticle dispersion ($\mu(FeO_x) = 0.12$ mass %) for 5 min in HEPES buffer at RT. Afterward, the cells are washed with HEPES buffer and fixed for TEM imaging with a 1% paraformaldehyde and 1.25% glutaraldehyde solution in cacodylate buffer (0.1 M pH 7.4) for one night at 4 °C. Fixation and embedding for TEM is carried out according to standard procedures.[28]

Results and Discussion

Functional Magnetic Core−Shell Nanoparticle Synthesis. Based on our recent results on the surface-engineering of superparamagnetic nanoparticles with polymer brush shells,[18,19,29,30] we developed a synthetic pathway to active ester-functional magnetic core shell nanoparticles. Starting from citrate-stabilized, highly magnetic iron oxide particles (FeO_x) in water, we modify the particle surface with an ATRP initiator. These macroinitiators are then used in the following surface initiated ATRP to result in magnetic hybrid particles.

More precisely, the synthesis of FeO_x nanoparticles is carried out by alkaline coprecipitation of iron(II) and iron(III) chloride leading to magnetic colloids with an average diameter of about 10.5 nm. The size reproducibility in this synthesis is as good as 5% for the number-average diameter, however, small differences in the size distribution give a higher deviation for the number-average value. By surface attachment of citric acid, a stabilization of the nanoparticles in water is obtained due to electrostatic repulsion.[31] Figure 1a shows a TEM image of the obtained small, spherical FeO_x nanoparticles.

To functionalize the nanoparticle surface with benzylic chlorine atoms for the initiation of ATRP, (p-chloromethyl)phenyltrimethoxysilane (CPTMS) is attached via ligand exchange to the particle surface and a cross-linked silica shell monolayer is formed, caging the magnetic core due to condensation of the silanol groups.[31] The initiator density is calculated from elemental analysis (EA) at 0.52 mmol·g^{-1} and 0.64 mmol·g^{-1}, respectively, for the two different batches employed in the following polymerization runs, indicating good conditions for an effective initiation and high grafting density.

OEGMA with an average number of ethylene glycol repeating units of 4.4 and methoxy end group ($M_n = 290$ g·mol^{-1}) is used as main monomer to generate a hydrophilic polymer shell that shows a critical solution behavior in water leading to magnetic polymer brushes with thermoresponsive dispersion behavior at around 65 °C. The biocompatibility of poly(ethylene glycol) derivates is helpful to obtain nanoparticles accepted for use in in vitro biological systems.

The direct introduction of carboxy functions to the polymer shell by surface-initiated ATRP involving (meth)acrylic acid is hindered by catalyst poisoning, resulting in a loss of reaction control.[29] To overcome this, the protection of the carboxy group is useful,[32] and in our approach, we employed succinimidyl methacrylate (SIMA) as a methacrylic acid derivative suitable for ATRP.[33−35] In model copolymerization experiments in solution, we proved the copolymerization behavior of the two monomers by analyzing the comonomer ratio and PDI at different stages of the polymerization. Comonomer conversion during polymerization was normally between 80 and 100%. The results of the copolymerization experiment are particularly important due to the fact that the respective hybrid particles are not accessible to solution NMR. The results are summarized in the Supporting Information. We found a constant comonomer ratio throughout the course of the reaction in all runs and a

Scheme 1. Synthesis of FeO_x−P(OEGMA-*co*-SIMA) Magnetic Polymer Brush Particles by Surface-Initiated ATRP

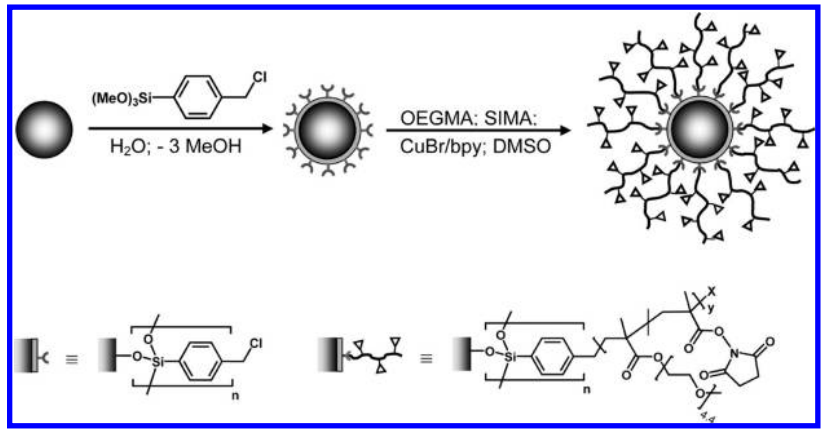

narrow molar mass distribution at SIMA contents <40 mol %. The copolymer composition is adjustable by the molar ratio of the monomers (Supporting Information). Furthermore, the succinimidyl ester function remains stable under the conditions of polymerization, as proven by NMR and IR, and can be used as an active ester in the amide formation for the nucleophilic attack of primary amines,[33−35] while OEGMA as the main comonomer determines the solution properties. For model copolymers up to 30 mol % SIMA fraction, we have found high water solubility and a lower critical solution behavior, in which the critical solution temperature T_c decreases with increasing SIMA content.

Magnetic polymer brush particles containing active ester units have been prepared by surface-initiated copolymerization of SIMA and OEGMA from CPTMS-modified FeO_x nanoparticles via ATRP in dimethylsulfoxide (DMSO; Scheme 1).

After 24 h, black viscous DMSO-based magnetic fluids are obtained. The success of the surface-initiated ATRP is qualitatively analyzed by transmission electron microscopy (TEM) and ATR-IR spectroscopy. A TEM image (Figure 1b) of the obtained nanoparticles visualizes strongly contrasting FeO_x cores surrounded by less contrasting polymer shells. The small nanoparticles are separately covered with a polymer layer of an average thickness of 3 nm independent of the core size.

ATR-IR spectra (Figure 2) of the dry FeO_x−P(OEGMA-*co*-SIMA) nanoparticles feature signals relating to the vibrational absorption of polymeric methyl and methylene groups (υ = 2800−3050 cm^{-1}), carbonyl double bond (υ = 1722 cm^{-1}), C−O deformation (υ = 1099 cm^{-1}), and N−O deformation (υ = 1025 cm^{-1}) clearly reveals the presence of P(OEGMA-*co*-SIMA). The three distinct peaks at υ = 1807, 1778, and 1722 cm^{-1} are characteristic of the vibrational absorption of the three carbonyl double bonds of the SIMA function, indicating that the succinimidyl ester is still existent and neither hydrolyzed nor deactivated.[33] From the carbon content obtained by elemental analysis (EA), a mass content of copolymer between 40 and 52 mass % is calculated (Table 1).

The hydrodynamic diameter of the core−shell nanoobjects in aqueous dispersion can be detected by dynamic light scattering (DLS). Compared to electrostatic stabilized particles and to CPTMS functionalized particles with a volume-average hydrodynamic diameter d_h of 19 and 26 nm, respectively, the size clearly increases for P(OEGMA-*co*-SIMA) coated nanoparticles to values between 47 and 79 nm, resulting from the formation of a polymer brush shell. It strikes that two of the runs, that is FeO_x−P(OEGMA-*co*-SIMA)25 and FeO_x−P(OEGMA-*co*-SIMA)15, show higher values for d_h in comparison to the other investigated samples, although the polymer fraction is not differing too much from the other batches. We assume the reason for that is the employment of a different initiator particle batch in these runs. As observed in VSM, the cores employed here show a higher volume-average diameter d_c compared to the other runs. The surface-modified particles thus provide a lower specific surface and, therefore, a lower specific initiator functionality (see above, at comparable initiation sites density of 4.9 $\mu mol \cdot m^{-2}$). At a similar polymer content, this results in longer chains being fixed on the cores with a weaker surface curvature and, therefore, leads to a higher hydrodynamic radius.

The quasi-static magnetic properties of FeO_x−P(OEGMA-*co*-SIMA) dispersions are investigated by vibrating sample magnetometry (VSM) experiments. Figure 3 shows a characteristic magnetization loop. The sigmoidal shape with low coercivity values (<0.6 $kA \cdot m^{-1}$) is attributed to superparamagnetic behavior of the core−shell nanoparticles. The saturation magnetization obtained from the experiments indicates a FeO_x

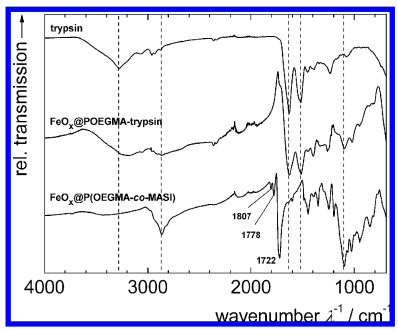

Figure 2. ATR-IR spectra of FeO_x−P(OEGMA-*co*-SIMA)25; trypsin, and trypsin-functional core−shell particles FeO_x−POEGMA-trypsin (dry powders).

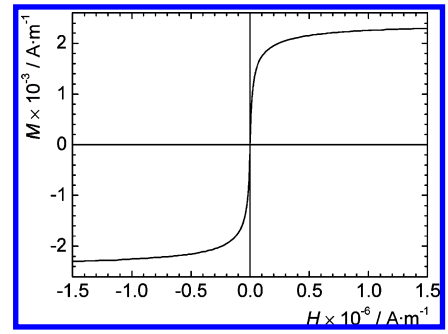

Figure 3. VSM loop of saturated magnetic fluid based on FeO_x−P(OEGMA-*co*-SIMA)15 nanoparticles in DMSO (μ_{MF} = 2.33 mass %).

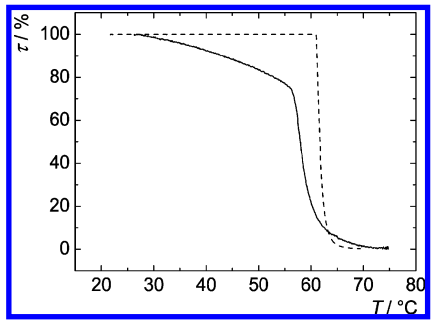

Figure 4. Relative transmittance τ vs temperature T of (partly hydrolyzed) FeO_x−P(OEGMA-*co*-SIMA)20 (compact line) and FeO_x−POEGMA (dashed line) suspensions in water in CPP experiments.

content between 1.5 and 2.3 mass %, according to the Langevin equation, and by using the initial susceptibility χ_{ini} from the graphs slope at $H = 0$, the volume-average core diameter can be calculated to values between 10.3 and 12.1 nm (Table 1).[36]

Zeta potential measurements on aqueous particle dispersions indicate low surface charges below +- 5 mV in a pH range between 3 and 8, and a poor pH dependence. The results therefore confirm the predominantly uncharged polymer shell in this pH range. However, when the pH is raised further, the zeta potential drops to −30 mV, indicating a hydrolysis of part of the active ester groups to carboxylate units in accordance to literature reports on the hydrolytic stability of *n*-succiminidyl esters.[24,25] (see Supporting Information).

In this context, the results of cloud point experiments performed on more concentrated particle dispersions as shown in Figure 4 have to be interpreted carefully. A sudden decrease in the relative transmittance τ is detected between 56 and 64 °C, caused by the increasing turbidity of the dispersion due to agglomeration and precipitation of the nanoparticles. This process is fully reversible and can be attributed to the lower critical solution temperature (LCST) of the OEGMA units of the polymer shell in water.[22] In contrast to what is found for model copolymers (see Supporting Information), the optically determined critical solution temperature T_c of the phase separation shows only a weak dependence on the initial SIMA content of the copolymer shell (see Table 1). As earlier results indicate, a similar thermoresponsive solution behavior of POEGMA derivatives immobilized on flat or nanoparticular surfaces as compared to linear soluted chains,[22,37,38] we attribute this to the occurrence of hydrolysis of a considerable part of the hydrophobic active ester groups during sample preparation.

In the agglomerated state above the LCST, simple permanent magnets with magnetic field gradients below 50 mT/cm are sufficient to separate the magnetic polymer brush particles from the carrier medium. We show below that this behavior is of use for the easy magnetic separation of amino-functional probes and magnetically labeled biomolecules. In this respect, it is of interest to note that the agglomeration temperature can be adjusted by copolymerization in a wide range including temperatures acceptable for biomolecules and biological species. We focus on this issue in our upcoming paper.

Determination of Particle Functionality by Amination. To investigate the (protected) COOH functionality and the binding capacity of FeO_x−P(OEGMA-*co*-SIMA) nanoparticles for primary amines, the capture of benzylamine (BzA) as a model substance from aqueous solution is examined. For this purpose, BzA solutions of different concentration are mixed with HEPES-buffered FeO_x−P(OEGMA-*co*-SIMA) particle dispersions and stirred at room temperature. In addition, a solution of 1-(3-dimethylaminopropyl)-3-ethylcarbodiimide hydrochloride (EDC) and *N*-hydroxysuccinimide (NHS) is added to reactivate hydrolyzed SIMA functions. On completion of the binding reaction overnight, the BzA functionalized nanoparticles are magnetically separated from the carrier medium at $T >$ LCST. There is no significant change of the LCST behavior observed due to BzA binding. The residual BzA in the carrier medium is quantified by ninhydrin reaction to Ruhemanns purple and subsequent detection by UV spectroscopy (Scheme 2).[39,40]

Figure 5a compares UV spectra of two supernatants and magnetic amine separation by FeO_x−P(OEGMA-*co*-SIMA)20 nanoparticles, and by FeO_x−POEGMA nanoparticles without active ester or carboxy groups in the polymeric shell, after ninhydrin reaction. As a reference, the UV spectrum of the basic 2.5 mM BzA solution after ninhydrin reaction without magnetic separation treatment is also shown. All spectra indicate the presence of the adduct by the presence of two absorption maxima at 400 and 568 nm for all samples. As evident, the spectra of the reference BzA solution and the BzA solution after magnetic separation with FeO_x−POEGMA nanoparticles are almost matching, indicating a comparable adduct concentration in both samples and, consequently, the absence of unspecific binding of BzA to the nano-objects that do not show active ester groups.

In contrast, when active ester bearing FeO_x−P(OEGMA-*co*-SIMA)20 nanoparticles are employed in the separation, the UV absorption after magnetic amine separation and ninhydrin reaction is significantly reduced in comparison to the reference solution.

After suitable calibration, the absorption at the peak maximum (568 nm) is used to extract the amount of residual BzA, $c_{r,BzA}$. We performed a representative experimental series and used the results to extract the particle functionality for three different runs of particles. By plotting $c_{r,BzA}$ versus the initial BzA concentration $c_{0,BzA}$, normalized by the magnetite concentration used for separation, c_{FeO_x} (Figure 5b), we observe linear graphs with an onset on the x coordinate that can be used to calculate the particles functionality.

For small initial BzA concentrations $c_{0,BzA}$, virtually no residual agent $c_{r,BzA}$ is detected, indicating that below a certain concentration nearly the full portion of BzA is captured by the particles. For BzA concentrations higher than this value, a sharp transition to a linear increase of $c_{r,BzA}$ with $c_{0,BzA}/c_{FeO_x}$, giving c_{FeO_x} as the slope, is detected. The intersections of the linear fits with the x-axis give the maximum amount of BzA that can be captured by the given content of hybrid particles. From the observed behavior, we may reasonably consider this value to be connected to the active ester functionality of the core−shell particles. For the investigated samples FeO_x−P(OEGMA-*co*-SIMA)20, FeO_x−P(OEGMA-*co*-SIMA)10, and FeO_x−P(OEGMA-*co*-SIMA)5, values for f of 29.5, 12.5, and 2.87 mmol·g^{-1} are obtained, reflecting the differing SIMA content in the polymeric shell resulting from the polymerization conditions. In contrast, commercially available, carboxy- or active ester bearing magnetic beads for magnetic separation typically show functionalities below 1 mmol·g^{-1}.[41] Owed to their brush-like architecture, our hybrid core shell nanoparticles possess a superior binding capacity of up to two scales higher, combined with quasi-homogeneous binding conditions in the highly solvated polymer shell, and easy magnetic separation above the LCST temperature.

Magnetic Biocatalysts by Enzyme Immobilization. The immobilization of biomacromolecules on magnetic carriers is of interest for separable biocatalytic systems. For a proof of principle study, we successfully immobilized trypsin as a model enzyme on the shell of FeO_x−P(OEGMA-*co*-SIMA)15 nano-

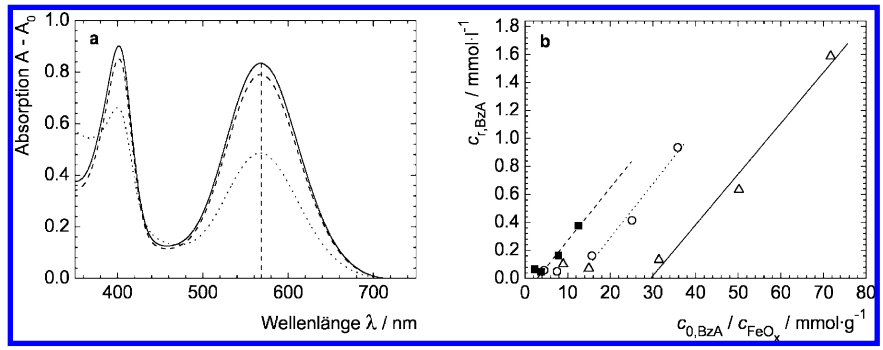

Figure 5. (a) UV spectra of residual BzA solution after ninhydrin reaction and magnetic amine separation by FeO_x−P(OEGMA-*co*-SIMA)20 (dotted line) and FeO_x−POEGMA (dashed line) nanoparticles in comparison to the primarily 2.5 mM BzA solution (compact line). (b) Concentration of residual BzA in solution $c_{r,BzA}$ after magnetic amine separation vs quotient of initial BzA concentration $c_{0,BzA}$ and FeO_x concentration c_{FeO_x}; open triangles (compact line): FeO_x−P(OEGMA-*co*-SIMA)20; open circles (dotted line): FeO_x−P(OEGMA-*co*-SIMA)10; solid squares (dashed line): FeO_x−P(OEGMA-*co*-SIMA)5.

Scheme 2. Quantification of Amine Separation by FeO_x−P(OEGMA-*co*-SIMA) Particles: (1) Separation of Magnetic Brush Particles at $T >$ LCST after Amination, and (2) Staining of Residual Amine in the Supernatant with Ninhydrin to Ruhemanns Purple and Quantification by UV Spectroscopy

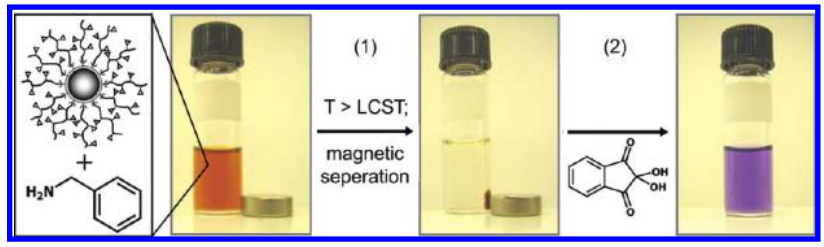

Scheme 3. Enzymatic Scission of BAPNA Catalyzed by Magnetically Labeled Trypsin ( )[a]

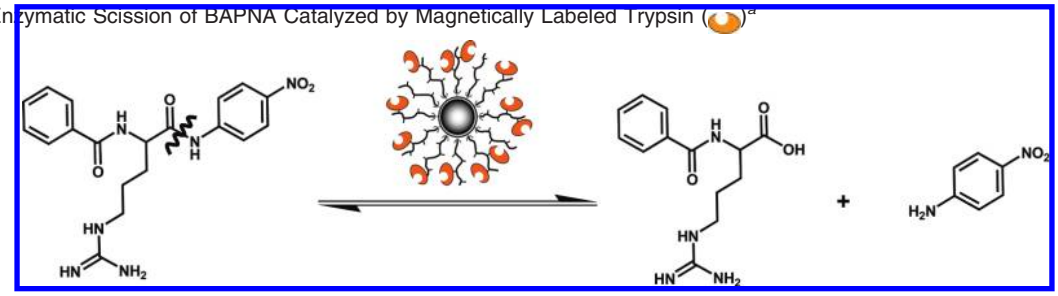

[a] The reaction product nitroaniline can be quantified spectroscopically.

particles. Particles with intermediate SIMA functionality have been chosen to ensure enough binding sites for amine capture, yet avoiding particle cross-linking or agglomeration due to multiple attachment of a single protein molecule by several nano-objects. Figure 2 compares the ATR-IR spectra of trypsin-functional nanoparticles FeO_x−POEGMA-trypsin to free trypsin. In both samples, we observe similar amide signals (υ = 1620, 1578 cm^{-1}), and also the NH-signal (υ = 3284 cm^{-1}) of the trypsin peptide sequence is visible in both spectra. From the nitrogen content obtained by EA, the amount of trypsin bound to the polymer surface of the nanoparticles is calculated to 1.1 $\mu mol \cdot g^{-1}$ or 26 $mg \cdot g^{-1}$. This loading is higher than that of commercially available magnetic particles for the protein binding with reported capacities between 1.5 $mg \cdot g^{-1}$ and 20 $mg \cdot g^{-1}$.[42] On the other hand, it is comparably lower than calculated from the active ester functionality of the hybrid particles reported above. We ascribe this to the different molecules size between BzA, employed for active ester group evaluation, and the protein, compared to the particle size and the proposed free volume between polymer chains. With a molar mass of 23300 $g \cdot mol^{-1}$, the molecule size of trypsin is in the same order as M_n of the surface immobilized polymer chains. Additionally, trypsin exhibits several amino groups within the protein sequence so that several active ester bearing polymer arms bind one trypsin molecule.

The catalytic activity of trypsin, a protease for hydrolysis of specific peptide bonds (chain scission after the amino acids arginine and lysine), is investigated for the particle-immobilized trypsin compared to free trypsin. For this purpose, we use the release of *p*-nitroaniline by the trypsin-mediated scission of N_α-benzoyl-D,L-arginine-4-nitroanilide (BAPNA) for the detection of the catalytic properties (Scheme 3).[43]

In our kinetic experiments concerning the trypsin-catalyzed scission reaction of BAPNA, the concentration of *p*-nitroaniline is followed throughout the reaction by UV spectroscopy at the absorption maximum of nitroaniline at 410 nm. An analogous set of experiments was carried out with native trypsin solution, as well as with FeO_x−POEGMA-trypsin (particle-immobilized trypsin) in aqueous dispersion (for details, see Experimental Section). As a control experiment, the primarily FeO_x−P(OEGMA-*co*-SIMA)15 nanoparticle dispersion without trypsin bound to the polymer shell is also used. Respective results for selected experiments are shown in Figure 6a.

In all runs employing either trypsin or immobilized trypsin, a linear increase of absorption with time can be detected in UV experiments, while the control does not react with BAPNA. To exclude possible trypsin leaching from the carriers, we continued the data collection for a couple of minutes after magnetic

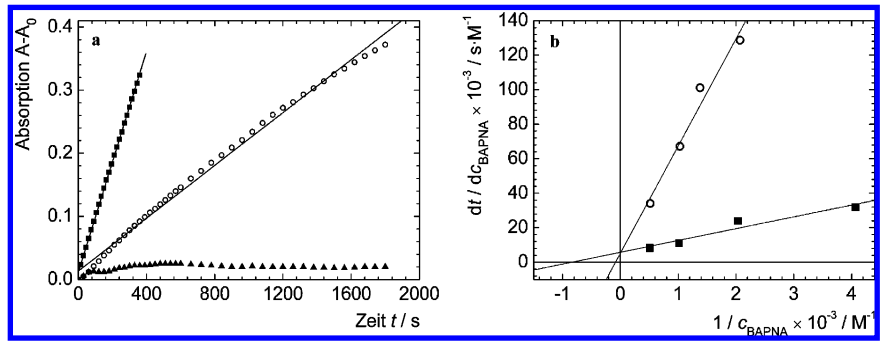

Figure 6. (a) UV absorption ($A-A_0$) at 410 nm over time t during reaction between BAPNA (2.0 mM) and FeO_x−POEGMA-trypsin nanoparticles (open circles) compared to free trypsin (solid squares) and FeO_x−P(OEGMA-*co*-SIMA)15 (solid triangles) nanoparticles. (b) Double-reciprocal plot of the rate of trypsin-catalyzed BAPNA scission, dc_{BAPNA}/dt, and the BAPNA concentration, c_{BAPNA}, according to Lineweaver and Burk; open circles: FeO_x−POEGMA-trypsin (c(trypsin) = 1.66 × 10^{-7} mol·L^{-1}); solid squares: free trypsin (c(trypsin) = 9.82 × 10^{-8} mol·L^{-1}).

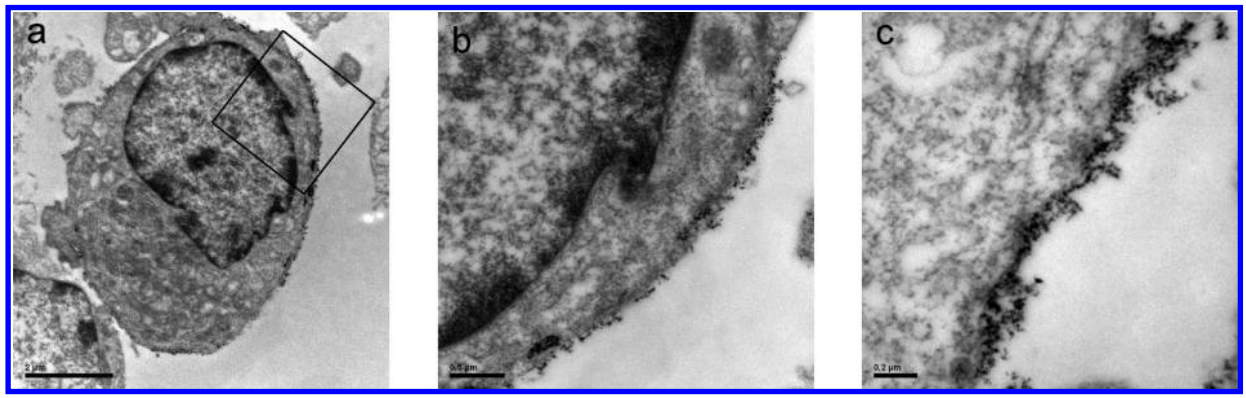

Figure 7. (a) TEM image of a human endothelial cell after incubation with FeO_x−P(OEGMA-*co*-SIMA)25 nanoparticles; (b) detail marked in (a) showing nanoparticles attached to the cell surface; (c) magnification of an endothelial cell surface efficiently coated with nanoparticles.

separation of FeO_x−POEGMA-trypsin nanoparticles from the BAPNA solution. No further increase in adsorption was detected.

The experiments have been performed with varying BAPNA c_{BAPNA} concentrations to obtain quantitative information on the kinetic parameters.[44] In Figure 6b, a double-reciprocal plot of the rate dc_{BAPNA}/dt is plotted against c_{BAPNA} according to Lineweaver and Burk.[45] The obtained linear relationship indicates that the trypsin-catalyzed scission of BAPNA follows a Michaelis−Menten mechanism for both free and immobilized trypsin. It is therefore possible to extract the kinetic parameters from the Michaelis−Menten equation:

$$v = v_{max}\frac{[S]}{K_M + [S]} \quad (1)$$

with v, conversion rate; v_{max}, maximum conversion rate (at infinite substrate concentration); K_M, Michaelis−Menten equilibrium constant; and [S], substrate concentration (here, c_{BAPNA}).

The determination of K_M and v_{max} for the two systems is done by the method of Eadie and Hofstee from a single-reciprocal plot of dc_{BAPNA}/dt against the quotient of dc_{BAPNA}/dt divided by c_{BAPNA}.[46−48] For free trypsin, K_M is calculated at 1.39 × 10^{-3} M and v_{max} at 2.11 × 10^{-4} M·s^{-1}, and for FeO_x−POEGMA-trypsin nanoparticles, K_M = 2.10 × 10^{-2} M and v_{max} = 3.45 × 10^{-4} M·s^{-1} for the respective trypsin concentration used in the experiment. To compare the enzymatic activity of free and immobilized trypsin, the maximum specific activity act_{spez}, given by the ratio of v_{max} and the trypsin concentration, was used in the experiment. We obtain a specific activity act_{spez} of 92.2 μmol·s^{-1}·mg^{-1} for free trypsin and 89.1 μmol·s^{-1}·mg^{-1} for immobilized trypsin, indicating no significant loss of enzyme activity upon immobilization. A likely explanation for the observed difference in the obtained Michaelis−Menten constant K_M is the hindered accessibility of the trypsin molecules bound to the polymer brush shell to its substrate molecules. This effect might be of even higher relevance for large molecules such as proteins and will be addressed in future experiments.

The active ester-functional FeO_x−P(OEGMA-*co*-SIMA) nanoparticles form covalent amide bonds with primary amines, and can thus be used to selectively label aminofunctional components of the exposed surface of a cell, for example, membrane proteins, to simplify their isolation and identification. To verify this concept, we performed labeling experiments of endothelial cell surface membranes. Cultured endothelial cells from human umbilical cord are incubated with FeO_x−P(OEGMA-*co*-SIMA)25 nanoparticles, and, as a control, with particles without binding sites for amino groups (FeO_x−POEGMA). In Figure 7, the successful binding is visualized by transmission electron microscopy (TEM). The surface of endothelial cells that has been exposed to a FeO_x−P(OEGMA-*co*-SIMA)25 dispersion shows an effective and dense labeling with nanoparticles after several washing steps. In contrast, nonfunctional FeO_x−POEGMA particles do not attach to the cell surface (Supporting Information).

Recently, we have shown that the labeled species can be magnetically separated and readily isolated after cell lysis. Digestion and identification of the species is subject to ongoing examination and beyond the scope of this paper.

Conclusion

The results demonstrate that by single-step surface-initiated copolymerization of active ester monomer SIMA with OEGMA,

brush-coated magnetic particles are obtained that possess a high number of accessible carboxy-analogue functional groups that can be further modified with bioactive species with the purpose of their manipulation or isolation. Here, we have shown that functional group densities of up to 30 mmol per gram of magnetite could be achieved that are accessible by small molecule substrates.

The particles are easily dispersed in aqueous media up to 23 mg/mL magnetite. The thermoreversible solvation of the shell is responsible for thermoflocculation, that results in a fast and highly effective magnetic isolation of the hybrid structures above the transition temperature.

As a result of the high functional group density, the particles show superior behavior in in vitro biocatalysis and labeling experiments. By immobilization of trypsin to the polymeric shell of the obtained nanoparticles, magnetically supported biocatalysts are obtained. Kinetic experiments on the catalytic activity via the trypsin mediated scission reaction of BAPNA reveal no loss in specific enzyme activity when compared to soluble trypsin. In addition, we have demonstrated the nanostructures' potential for selective tagging and separation of the exposed surface of endothelial cells in order to facilitate the isolation and identification of membrane proteins. While unspecific adsorption of nonfunctional particles was not observed, in vitro experiments involving active ester group bearing core−shell particles resulted in a dense population of particles at the exposed cell membrane, attributed to the formation of covalent (amide) bonds.

The principle described here is applicable to the modification with other biologically or catalytically relevant groups and will therefore open new ways for the design of multifunctional hybrid nanostructures with different property portfolios.

Acknowledgment. We thank Prof. H. Ritter for his steady interest in our studies. Thanks to Dr. B. Emde for her support with biological and technical questions. We thank Dr. Yan Lu University of Bayreuth (Germany) for TEM images of the particles. We gratefully acknowledge DFG for financial support within the Emmy-Noether Program and the Priority Program SPP 1259.

Supporting Information Available. Synthesis and properties of P(OEGMA-*co*-SIMA) model copolymers, zeta potential measurements, and TEM of cell labeling control experiment. This material is available free of charge via the Internet at http://pubs.acs.org.

References and Notes

(1) Horák, D.; Babiè, M.; Macková, H.; Beneš, M. J. *J. Sep. Sci.* **2007**, *30*, 1751–1772.
(2) Gu, H.; Xu, K.; Xu, C.; Xu, B. *Chem. Commun.* **2006**, 941–949.
(3) Franzrep, M.; Siemann-Herzberg, M.; Hobley, T. J.; Thomas, O. R. T. *Appl. Microbiol. Biotechnol.* **2006**, *70*, 505–516.
(4) Safarik, I.; Safarikova, M. *BioMagn. Res. Technol.* **2004**, *2*, 1–17.
(5) Pankhurst, Q. A.; Connolly, J.; Jones, S. K.; Dobson, J. *J. Phys. D: Appl. Phys.* **2003**, *36*, R167–R181.
(6) Safarik, I.; Safarikova, M. *J. Chromatogr., B* **1999**, *722*, 33–53.
(7) Yalcýn, A.; Damin, F.; Ozkumur, E.; di Carlo, G.; Goldberg, B. B.; Chiari, M.; Unlu, M. S. *Anal. Chem.* **2009**, *81*, 625–630.
(8) Kondo, A.; Kamura, H.; Higashitani, K. *Appl. Microbiol. Biotechnol.* **1994**, *44*, 99–105.
(9) Lai, J. J.; Hoffman, J. M.; Ebara, M.; Hoffman, A. S.; Estourne's, C.; Wattiaux, A.; Stayton, P. S. *Langmuir* **2007**, *23*, 7385–7391.
(10) Sun, Y.; Ding, X.; Zheng, Z.; Cheng, X.; Hu, X.; Peng, Y. *Chem. Commun.* **2006**, 2765–2767.
(11) Ohnishi, N.; Furukawa, H.; Hideyuki, H.; Wang, J.-M.; An, C.-I.; Fukusaki, E.; Kataoka, K.; Ueno, K.; Kondo, A. *BioNanotechnology* **2006**, *2*, 43–49.
(12) http://www.magnabeat.com/e_index.html.
(13) Perruchot, C.; Khan, M. A.; Kamitsi, A.; Armes, S. P.; von Werne, T.; Patten, T. E. *Langmuir* **2001**, *17*, 4479–4481.
(14) Chen, X. Y.; Randall, D. P.; Perruchot, C.; Watts, J. F.; Patten, T. E.; von Werne, T.; Armes, S. P. *J. Colloid Interface Sci.* **2003**, *257*, 56–64.
(15) Li, D.; Sheng, X.; Zhao, B. *J. Am. Chem. Soc.* **2005**, *127*, 6248–6256.
(16) Li, D.; Jones, G. L.; Dunlap, J. R.; Hua, F.; Zhao, B. *Langmuir* **2006**, *22*, 3344–3351.
(17) Schmidt, A. M. *Macromol. Rapid Commun.* **2005**, *26*, 93–97.
(18) Gelbrich, T.; Feyen, M.; Schmidt, A. M. *Macromolecules* **2006**, *39*, 3469–3472.
(19) Kaiser, A.; Gelbrich, T.; Schmidt, A. M. *J. Phys.: Condens. Matter* **2006**, *18*, 2563–2580.
(20) Wang, S.; Zhou, Y.; Guan, W.; Ding, B. *Appl. Surf. Sci.* **2008**, *254*, 5170–5174.
(21) Gou, Z.; Chen, Y.; Zhou, W.; Huang, Z.; Hu, Y.; Wan, M.; Bai, F. *Mater. Lett.* **2008**, *62*, 4542–4544.
(22) Chanana, M.; Jahn, S.; Georgieva, R.; Lutz, J.-F.; Bäumler, H.; Wang, D. *Chem. Mater.* **2009**, *21*, 1906–1914.
(23) Lutz, J.-F.; Stiller, S.; Hoth, A.; Kaufner, L.; Pison, U.; Cartier, R. *Biomacromolecules* **2006**, *7*, 3132–3138.
(24) Murata, H.; Prucker, O.; Rühe, J. *Macromolecules* **2007**, *40*, 5497–5503.
(25) Cullen, S. P.; Mandel, I. C.; Gopalan, P. *Langmuir* **2008**, *24*, 13701–13709.
(26) Batz, H.-G.; Franzmann, G.; Ringsdorf, H. *Angew. Chem.* **1972**, *24*, 1189–1190.
(27) Massart, R.; Cabuil, V. *J. Chem. Phys.* **1987**, *84*, 967–973.
(28) Schimmel, G., Vogell, W., Eds. *Methodensammlung der Elektronenmikroskopie*; Wissenschaftliche Verlagsgesellschaft mbH: Stuttgart, 1983.
(29) Kaiser, A.; Schmidt, A. M. *J. Phys. Chem. B* **2008**, *112*, 1894–1998.
(30) Gelbrich, T.; Feyen, M.; Schmidt, A. M. *Z. Phys. Chem.* **2006**, *220*, 41–49.
(31) Frickel, N.; Messing, R.; Gelbrich, T.; Schmidt, A. M. *Langmuir* **2009**, DOI: 10.1021/la902904f.
(32) Matyjaszewski, K.; Davis, T. P. *Handbook of Radical Polymerization*; WileyIntersience: New York, 2002.
(33) Rathforn, J. M.; Tew, G. N. *Polymer* **2008**, *49*, 1761–1769.
(34) Shunmugam, R.; Tew, G. N. *J. Polym. Sci., Part A: Polym. Chem.* **2005**, *43*, 5831–5843.
(35) Monge, S.; Haddelton, D. M. *Eur. Polym. J.* **2004**, *40*, 37–45.
(36) Odenbach, S. *Magnetoviscous Effects in Ferrofluids*; Springer-Verlag, 2002.
(37) Jones, A. M.; Glinel, K.; Oren, R.; Nysten, B.; Huck, W. T. S. *Macromolecules* **2007**, *40*, 4403–4405.
(38) Lutz, J.-F.; Hoth, A. *Macromolecules* **2006**, *39*, 893–896.
(39) Sarin, K. V.; Kent, S. B. H.; Tam, J. P.; Merrifield, R. B. *Anal. Biochem.* **1981**, *117*, 147–157.
(40) McCaldin, D. J. *Chem. Rev.* **1960**, *60*, 39–51.
(41) www.ademtech.com, adembeads, $f = 0.35$ mmol·g^{-1}; www.bangslabs.com, BioMag, $f = 0.24$ mol·g^{-1}; www.chemagen.de, M-PVA Magnetic beads activated AK11, $f = 0.39$ mmol·g^{-1}; www.invitrogen.com, Dynabeads MyOne, $f = 0.4-0.8$ mmol·g^{-1}.
(42) www.chemagen.de,M-PVA Magnetic beads activated AK11 protein binding capacity, 8−20 mg·g^{-1}; www.micromod.de, nanomag-D (streptavidin) streptavidin functionality, 1.5−2.0 mg·g^{-1}.
(43) Erlanger, B. F.; Kokowsky, N.; Cohen, W. *Arch. Biochem. Biophys.* **1961**, *95*, 271–278.
(44) Michaelis, L.; Menten, M. L. *Biochem. Z.* **1913**, *49*, 333–369.
(45) Lineweaver, H.; Burk, D. *J. Am. Chem. Soc.* **1934**, *56*, 658–666.
(46) Hofstee, B. H. J. *Nature* **1959**, *184*, 1296–1298.
(47) Hofstee, B. H. J. *Science* **1952**, *116*, 329–331.
(48) Eadie, G. S. *J. Biol. Chem.* **1942**, *146*, 85–93.

BM901203Z